Inorganic Chemistry

Article

pubs.acs.org/IC

Self-Assembly of Extended Head-to-Tail Triangular Pt_3 Macrocycles into Nanotubes

Zhengyu Chen, Brian J. Sahli, and Mark J. MacLachlan*

Department of Chemistry, University of British Columbia, 2036 Main Mall, Vancouver, British Columbia V6T 1Z1, Canada

Supporting Information

ABSTRACT: New pyridylsalicylaldimine-based ligands with extended conjugation have been synthesized. The reaction of these ligands with K_2PtCl_4 yielded triangular Pt_3 macrocycles rather than the anticipated Pt_4 macrocycles. The macrocycles have been analyzed in solution by variable-temperature and variable-concentration ^1H NMR, NOESY, and DOSY spectroscopy studies. These investigations show that the macrocycles aggregate at room temperature in solution by an entropy-driven process. In the solid state, matrix-assisted laser desorption/ionization time-of-flight mass spectrometry and transmission electron microscopy studies show that the macrocycles aggregate into nanotubular structures. Triangular platinum-containing macrocycles with the expanded pyridylsalicylaldimine ligands are promising for constructing nanotubes and discotic liquid crystals.

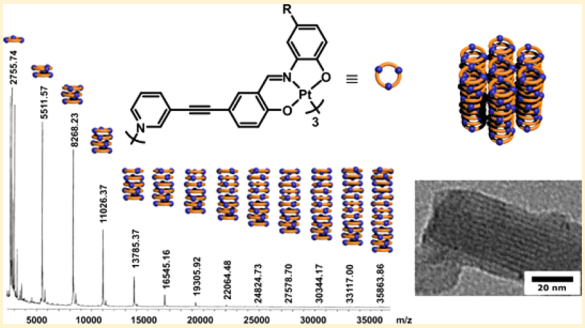

INTRODUCTION

Supramolecular chemistry, where intermolecular interactions are used to organize structures,[1] is a powerful paradigm in the synthesis of complex substances such as metal−organic frameworks,[2] catenanes,[3] and gels.[4] Macrocycles have had a prominent role in the development of the field of supramolecular chemistry, perhaps most notably Pederson's development of crown ethers.[5] Shape-persistent macrocycles[6] have been investigated for several decades and have already attracted significant attention for developing new functional materials, such as liquid crystals,[7] nanofibers,[8] and ion channels.[9] They are also of interest for exploring new concepts in host−guest chemistry[10] and self-assembly.[11]

Among those properties, the self-assembly of shape-persistent macrocycles into nanoscale structures has been extensively pursued.[12] Many organic macrocycles have been investigated as building blocks to form tubular assemblies upon stacking with the goal of developing new families of molecule-based nanotubes.[13] Forming tubular structures by stacking cyclic building blocks has some inherent advantages over other methods of constructing nanotubes. For example, the size and shape of the macrocycles can be readily modified, leading to tunable and predictable cavity sizes for the resulting nanotubes.[14] Furthermore, the properties of the inside or outside of the nanotubes may be modified by changing the internal or side-chain functionalities, respectively, during the synthesis of macrocycles. This could allow for control of the hydrophobicity,[15] metal binding ability,[16] and reactivity, for instance.

The stacking of shape-persistent macrocycles into nanotubes may be facilitated by weak $\pi-\pi$ interactions[17] (which are largely driven by desolvation of the rings upon stacking) or hydrogen bonding.[18] Ghadiri and co-workers constructed artificial membrane ion channels from self-assembling peptide nanotubes.[19] Moreover, Gong's group developed a family of oligoamide macrocycles for spontaneous self-assembly into nanotubes that can serve as highly conductive transmenbrane channels.[20] Other examples abound in the literature.[21]

In 2010, we reported new platinum-containing macrocycles that are constructed from a head-to-tail assembly (Scheme S1).[22] In each case, only the Pt_4 macrocycle was observed by mass spectrometry, with no evidence of forming either smaller or larger rings. These macrocycles can self-assemble into columnar structures by $\pi-\pi$ stacking. Interestingly, by using large substituents, it was possible to isolate discrete hexamers and tetramers of the Pt_4 macrocycles in the solid state.[23] We set out to extend the organic linker in order to make larger Pt_4 macrocycles, so that they would have better guest-accessible channels for exploring their supramolecular chemistry. We believed that the geometry of the ligand was robust and that extending the distance between the platinum salicylaldehyde groups while maintaining the geometry of the structure would lead to larger Pt_4 macrocycles.

In this paper, we report our investigations of platinum-containing macrocycles with extended conjugated ligands based on the pyridylsalicylaldehyde system. We describe their aggregation behavior in the solid state and solution as probed by many techniques.

EXPERIMENTAL SECTION

Materials and Equipment. All reactions were carried out under air unless otherwise stated. Tetrahydrofuran was distilled from

Received: February 21, 2017

DOI: 10.1021/acs.inorgchem.7b00475
Inorg. Chem. XXXX, XXX, XXX−XXX

sodium/benzophenone under nitrogen. Diisopropylamine was distilled from NaOH under nitrogen. Acetonitrile, methanol (MeOH), and triethylamine were purged with nitrogen gas and dried over molecular sieves before use. All reagents were used as received unless otherwise stated. ^{1}H and ^{13}C{^{1}H} NMR spectra were recorded on either a Bruker AV-300 or a Bruker AV-400 spectrometer. Mass spectrometry (MS) data and elemental analyses were obtained at the Microanalytical Services Laboratory, University of British Columbia. Matrix-assisted laser desorption/ionization (MALDI) MS spectra were obtained on a Bruker Biflex IV time-of-flight (TOF) mass spectrometer equipped with a MALDI ion source. Electrospray ionization (ESI-)MS spectra were obtained on a Bruker Esquire-LC ion-trap mass spectrometer equipped with an electrospray ion source. High-resolution electrospray ionization (HR-ESI) MS spectra were obtained on a Micromass LCT TOF mass spectrometer equipped with an electrospray ion source. Gramicidin S, Rifampicin, and Erythromycin were used as the references for HR-ESI. Elemental analyses were obtained on a Carlo Erba EA 1108 elemental analyzer. Melting points were obtained on a Fisher-John's melting point apparatus. IR spectra were obtained using a Thermo Scientific Nicolet 6700 FT-IR spectrometer equipped with a diamond attenuated-total-reflectance accessory. UV−vis spectra were obtained in chloroform on a Varian Cary 5000 UV−vis−near-IR spectrophotometer using a 1 cm quartz cuvette. For transmission electron microscopy (TEM) studies, macrocycle **1a** was suspended in ethanol, and the suspension was then transferred onto a copper TEM grid and placed in the oven at 333 K to dry. TEM was performed on a Hitachi H7600 transmission electron microscope.

*Synthesis of Macrocycle **1a**.* A suspension of K_2PtCl_4 (58 mg, 0.14 mmol) in dimethyl sulfoxide (DMSO; 8 mL) was sparged with nitrogen and then heated to 100 °C until all of the salt dissolved. A separate Schlenk flask was charged with imine **2a** (0.10 g, 0.14 mmol) and K_2CO_3 (48 mg, 0.35 mmol), and two cycles of evacuation/N_2 purging were conducted. The K_2PtCl_4 solution was transferred via a syringe to the flask containing imine and K_2CO_3, and the mixture was then heated at 120 °C for 6 h. The yellow-brown suspension was cooled to room temperature, followed by centrifugation. After the supernatant solution was decanted, three cycles of washing, centrifuging, and decanting were performed, once with water and twice with MeOH. Upon drying of the precipitate, the macrocycle was isolated as a yellow powder (49 mg, 0.018 mmol, 39%). ^{1}H NMR (400 MHz, $CDCl_3$, 25 °C): δ 8.74 (br s, 1H), 8.57 (br s, 1H), 7.64 (br s, 1H), 7.15−7.42 (m, 16H), 7.13 (br s, 1H), 6.89 (d, J = 8.0 Hz, 1H), 6.61 (d, J = 8.0 Hz, 1H), 6.23 (br s, 1H), 1.39 (s, 27H). ^{13}C{^{1}H} NMR (400 MHz, $CDCl_3$): δ 166.2, 162.0, 148.8, 148.6, 146.3, 144.7, 139.7, 139.0, 136.4, 136.1, 135.4, 134.2, 132.1, 131.0, 124.2, 123.9, 122.8, 122.0, 117.6, 116.8, 109.9, 95.8, 84.4, 63.2, 34.4, 31.5 (missing one peak). IR: ν 3083, 3031, 2958, 2903, 2869, 2206, 1596, 1571, 1492, 1415, 1380, 1362, 1316, 1269, 1195, 1135, 1109, 1064, 1017, 916, 818, 708, 688 cm^{-1}. MALDI-TOF MS: m/z 2755.7 ([M + H]$^+$). Mp: >360 °C.

*Synthesis of Macrocycle **1b**.* A suspension of K_2PtCl_4 (146 mg, 0.351 mmol) in DMSO (20 mL) was sparged with nitrogen and then heated to 100 °C until all of the salt dissolved. A separate Schlenk flask was charged with imine **2b** (290 mg, 0.351 mmol) and K_2CO_3 (97 mg, 0.70 mmol), and two cycles of evacuation/N_2 purging were conducted. The K_2PtCl_4 solution was transferred via a syringe to the flask containing imine and K_2CO_3, and the mixture was heated at 120 °C for 6 h. The yellow-brown suspension was cooled to room temperature, followed by centrifugation. After decanting the supernatant solution, three cycles of washing, centrifuging, and decanting were performed, once with water and twice with MeOH. Upon drying of the precipitate, the macrocycle was isolated as a yellow powder (136 mg, 0.0445 mmol, 38%). IR: ν 3083, 3031, 2960, 2904, 2869, 2201, 1596, 1508, 1489, 1409, 1363, 1314, 1269, 1197, 1175, 1135, 1018, 918, 820, 709, 685 cm^{-1}. MALDI-TOF MS: m/z 3055.88 ([M + H]$^+$). Mp: >360 °C.

*Synthesis of Model Compound **1c′**.* A suspension of K_2PtCl_4 (52 mg, 0.12 mmol) in DMSO (6 mL) was sparged with nitrogen and then heated to 100 °C until all of the salt dissolved. A separate Schlenk flask was charged with imine **2c** (90 mg, 0.12 mmol) and K_2CO_3 (34 mg, 0.25 mmol), and two cycles of evacuation/N_2 purging were conducted. The K_2PtCl_4 solution was transferred via a syringe to the flask containing imine and K_2CO_3, and the mixture was heated at 150 °C for 4 h. The yellow-brown suspension was cooled to room temperature, followed by centrifugation. After the supernatant solution was decanted, three cycles of washing, centrifuging, and decanting were performed, once with water and twice with MeOH. Upon drying of the precipitate, the macrocycle was isolated as a yellow powder (28 mg, 0.028 mmol, 23%). ^{1}H NMR (400 MHz, $CDCl_3$, 25 °C): δ 9.19 (m, 2H), 8.11 (s, 1H), 7.95 (tt, J = 8.0(2) and 1.8(2) Hz, 1H), 7.63 (d, J = 2.0 Hz, 1H), 7.55 (dd, J = 8.8 and 2.0 Hz, 1H), 7.46−7.53 (m, 5H), 7.31−7.36 (m, 3H), 7.28−7.31 (m, 6H), 7.18−7.21 (m, 6H), 7.15−7.18 (m, 1H), 6.96−7.01 (m, 2H), 1.35 (s, 27H). ^{13}C{^{1}H} NMR (400 MHz, $CDCl_3$): δ 165.7, 162.0, 149.9, 148.5, 144.1, 142.4, 138.8, 138.4, 137.5, 135.5, 135.1, 132.8, 131.3, 130.8, 128.3, 127.7, 125.2, 124.1, 123.8, 122.2, 121.8, 117.2, 116.3, 111.0, 89.2, 87.8, 63.1, 34.4, 31.4 ppm. IR: ν 2963, 2902, 2867, 2212, 1671, 1606, 1595, 1494, 1484, 1375, 1314, 1271, 1177, 1018, 922, 840, 822, 757, 687 cm^{-1}. ESI-MS (MeOH). Calcd: m/z 996.4 ([M + H]$^+$). Found: m/z 996.5. Mp: >360 °C. Anal. Calcd for $C_{57}H_{56}N_2O_2Pt$: C, 68.73; H, 5.67; N, 2.81. Found: C, 69.03; H, 5.71; N, 2.83.

■ RESULTS AND DISCUSSION

In an effort to prepare Pt_4 macrocycles **1a′** and **1b′** (Figure 1) with expanded diameters, we first constructed compounds **3a** and **3b** (Scheme 1) by Sonogashira coupling of acetylene derivatives to aryl halides. Ligands **2a** and **2b** were prepared by condensing aminophenol **6** with **3a** and **3b**, respectively. The bulky substituents were selected to inhibit aggregation of the macrocycles and improve their solubility so that they could be studied in solution. Importantly, these new ligands have the same overall geometry as the ligands used previously to prepare the Pt_4 macrocycles in Scheme S1 in terms of the orientation of the pyridyl nitrogen with respect to the salicylaldehyde.

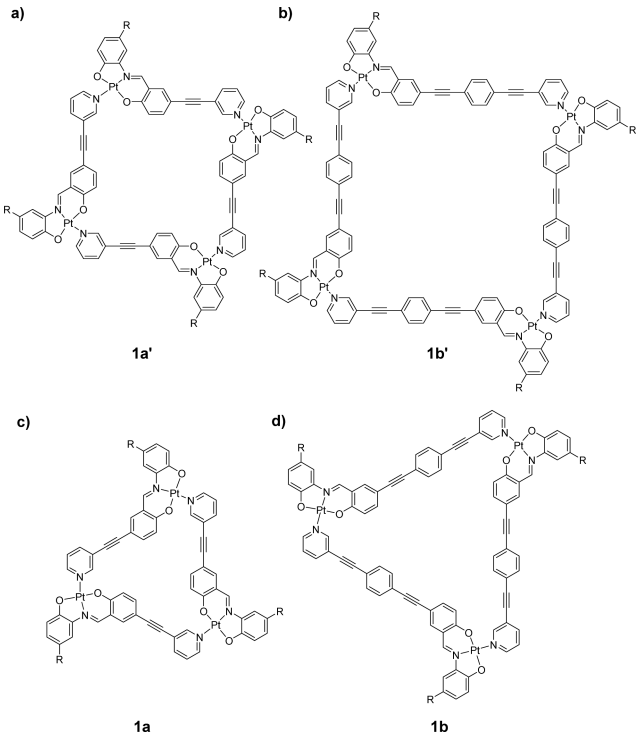

Figure 1. (a and b) Structures of the target extended macrocycles **1a′** and **1b′** anticipated in this study (not obtained). (c and d) Structures of the Pt_3 macrocycles **1a** and **1b** obtained in this study.

DOI: 10.1021/acs.inorgchem.7b00475
Inorg. Chem. XXXX, XXX, XXX−XXX

Scheme 1. Syntheses of (a) Aminophenol 6, (b) Ligand 2a and Macrocycle 1a, and (c) Ligand 2b and Macrocycle 1b

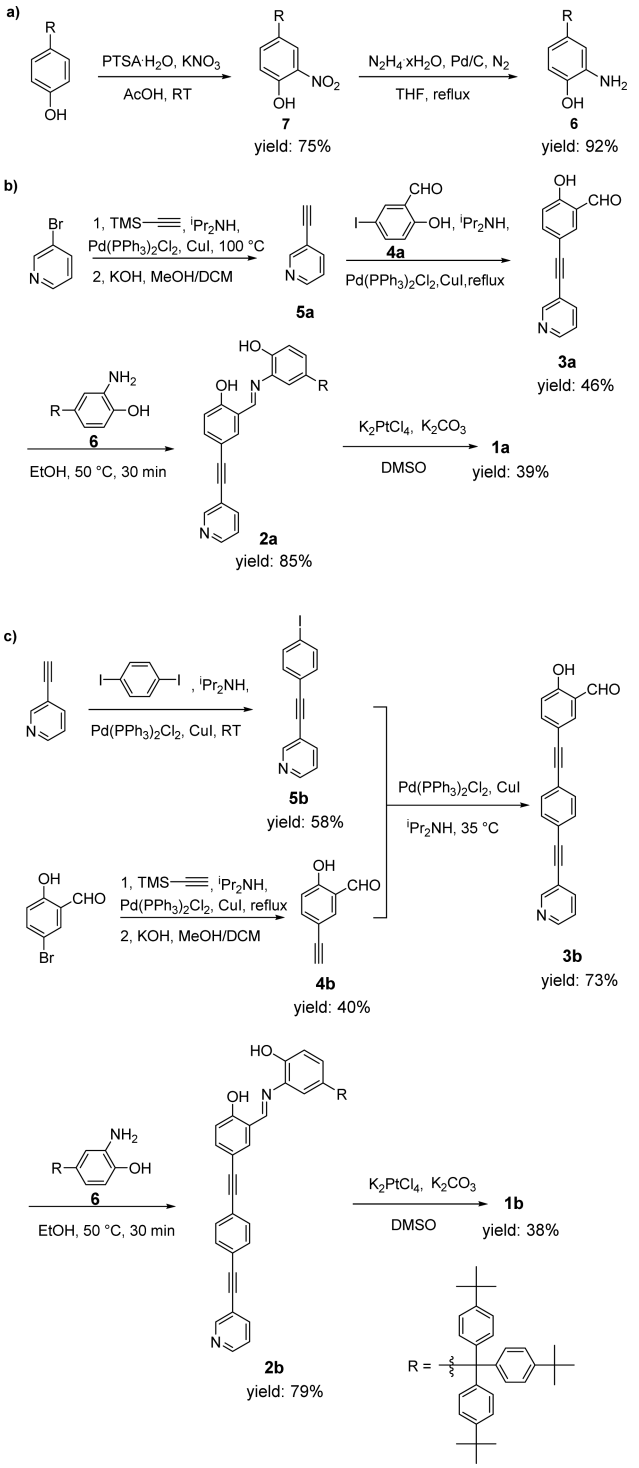

Consequently, we expected that the reaction of these new ligands with Pt^{2+} salts would afford Pt_4 macrocycles **1a′** and **1b′**.

The reaction of **2a** with K_2PtCl_4 gave a yellow powder. MALDI-TOF MS of the product revealed that the product was not the intended Pt_4 macrocycle **1a′** (MW = 3670.4 g/mol) but rather Pt_3 macrocycle **1a** (MW = 2754.1 g/mol) (Figure 2).[24] Also, MALDI-TOF MS showed aggregates of the Pt_3 macrocycle, suggesting that the macrocycles have a strong tendency to stack (as previously observed with the Pt_4 macrocycles).

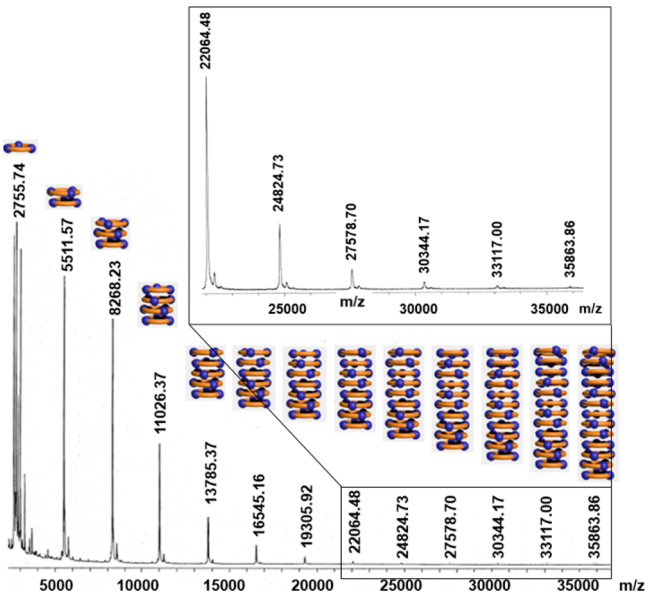

Figure 2. MALDI-TOF MS of macrocycle **1a**. The peak at m/z 2755.7 corresponds to that of the protonated Pt_3 macrocycle, $[\mathbf{1a}+H]^+$.

Surprisingly, Pt_3 rings were exclusively obtained with the expanded ligand **2a**. The change of the geometry can be explained by two factors. First, the insertion of acetylene groups introduced flexibility to the organic linkers.[25] The additional flexibility could contribute to the formation of macrocycles with unexpected geometry.[26] Second, in our previous organic linker containing pyridyl-substituted salicylaldehyde, the ground-state conformation of the ligand has a torsion between the two aromatic rings. This nonplanarity may favor the square-shaped macrocycle, whereas in **1a** and **1b**, the ligands can adopt a conformation where the pyridyl and salicylaldimine components are coplanar. Thus, the flat conformation of the macrocycle may favor the triangular macrocycles. The enhanced planarity of macrocycle **1a** may lead to enhanced stacking. These results suggest that macrocycle **1a** has excellent potential for supramolecular assembly into nanotubes. As noted in Figure 2, MALDI-TOF MS shows a strong stacking pattern for macrocycle **1a**. In fact, we could observe up to 13 macrocycles stacked together. Qualitatively, macrocycle **1a** appears to be more prone to stacking than the Pt_4 macrocycles with the same substituents.

A computational study was conducted to investigate the macrocycle conformation. To simplify the system, a Pt_3 macrocycle with R = H was used as a model compound (Figure 3). The geometry was optimized using the density functional theory (DFT) PBE0 exchange-correlation functional, with the LANL2DZ core potential and basis set for platinum and the 6-31g(d) basis set for all other atoms. This level of theory is commonly chosen for complexes of iridium, palladium, and platinum based on favorable comparisons with gas-phase and high-level ab initio structural data.[27] In the optimized conformation, all three repeating units have similar bond and twisting angles. Overall, the optimized conformation of the macrocycle is almost planar, but it bends very slightly to one side to give a shallow bowl-shaped conformation.

DOI: 10.1021/acs.inorgchem.7b00475
Inorg. Chem. XXXX, XXX, XXX−XXX

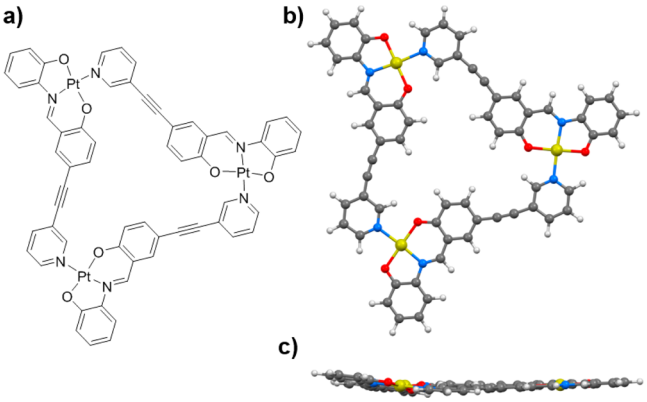

Figure 3. (a) Chemical structure of Pt_3 macrocycle **1a** with R = H. (b) Top and (c) side views of the DFT-optimized geometry of the macrocycle with R = H, computed at the PBE0/LANL2DZ(Pt) and 6-31g(d) (other atoms) levels of theory.

All C≡C triple bonds in the organic linkers showed a C—C≡C bond angle of about 6°. The extra flexibility introduced by acetylene groups contributed to the formation of the 3-fold-symmetric macrocycle. In addition, in the calculated structure, two aromatic rings belonging to the same organic linker almost stay in the same plane, where they can maximize conjugation. In fact, all of the aromatic rings from the same Pt_3 macrocycle are nearly coplanar. The flattened conformation of the organic linkers with flexible acetylene groups allowed the triangular macrocycle to form.

Another Pt_3 macrocycle **1b** was prepared by a similar approach from **2b**, and MALDI-TOF MS verified that it was also the Pt_3 macrocycle that predominated in the product. However, macrocycles with other geometries could also be observed in the MALDI-TOF MS spectrum as minor products. Moreover, strong stacking was not observed in this case. Notably, macrocycle **1b** showed much weaker signals in the MALDI-TOF MS spectrum compared to macrocycle **1a**. Because macrocycle **1b** demonstrated very poor solubility in organic solvents, macrocycle **1a** was chosen for the following self-assembly studies.

The MALDI-TOF MS data for macrocycle **1a** suggested that it aggregates strongly in the solid state. More experiments were performed to investigate the self-assembly. Unfortunately, attempts to grow a single crystal of macrocycle **1a** were unsuccessful. Powder X-ray diffraction (PXRD) of macrocycle **1a** showed no sharp diffraction peaks beyond $2\theta = 5°$ (Figure S23). However, a peak was evident at $2\theta = 3.75°$ (23.5 Å *d* spacing), suggesting a higher-order organization within the substance. We felt that this could arise from columnar stacking of the macrocycles in the solid state. Because the typical pattern of columnar stacks of disklike molecules is usually a hexagonal lattice,[28] the diameter of the macrocycles can be calculated from the 23.5 Å *d* spacing as 2.71 nm, which is consistent with the estimated diameter of macrocycle **1a**.

To corroborate this interpretation, TEM studies of macrocycle **1a** were undertaken. Stripes with an average separation of about 2.6 nm are clearly evident in the TEM images (Figure 4). This value is close to the diameter estimated for a stacked macrocycle nanotube and the PXRD result. Thus, we believe that the TEM images show that the macrocycles have stacked one on top of the other into a nanotubular structure, which is organized into a hexagonal lattice. This organization is reminiscent of the Pt_4 macrocycles, which also stacked into columns in the solid state. The proposed model of the solid-state organization of **1a** is shown in the inset of Figure 4.

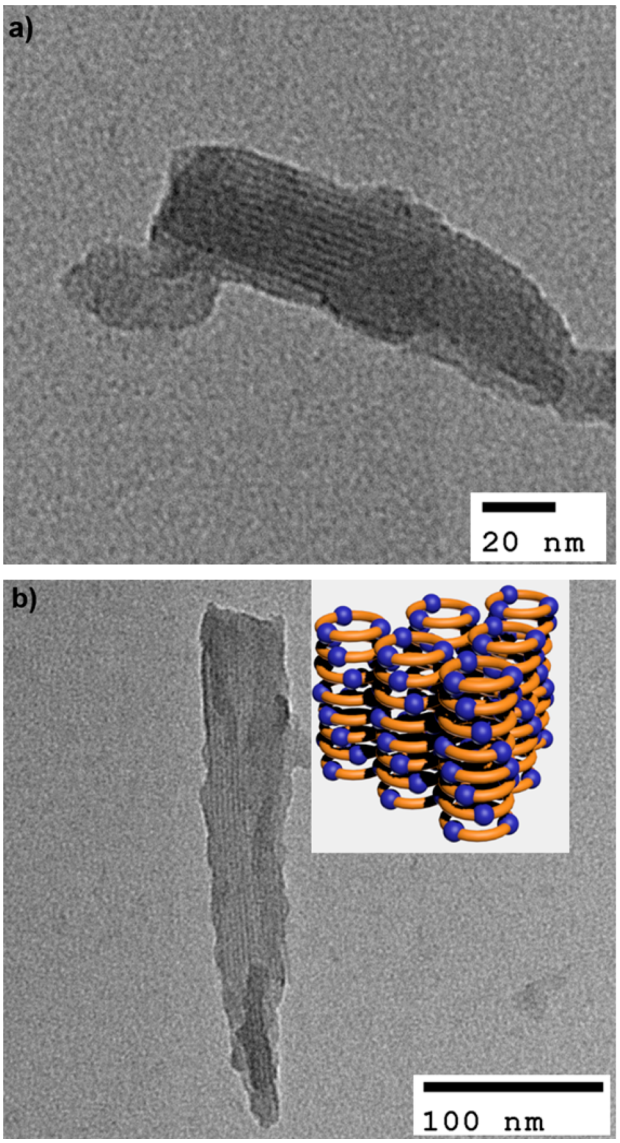

Figure 4. TEM images of macrocycle **1a**. The repeating distance between adjacent stripes is approximately 2.6 nm, and the inset shows the proposed organization of **1a** in the solid state.

The actual stacking structure of the macrocycles is likely disordered. When a head-to-tail macrocycle stacks on top of another one, the second macrocycle could stack with either the same or opposite orientation as the first molecule (Figure S24). Within a long stack, the possibility of different relative orientations between adjacent macrocycles will lead to a large number of possible stacks and, consequently, substantial disorder. This stacking disorder might be the reason for the lack of sharp peaks in the PXRD pattern of macrocycle **1a**.

Although it was shown that Pt_3 macrocycle **1a** self-assembles in the solid state, its behavior in solution remained unknown. Therefore, we conducted NMR experiments to study its behavior in solution. Because of the macrocycle's poor solubility in most organic solvents, NMR experiments were only conducted in $CDCl_3$. The ^1H NMR spectrum of macrocycle **1a** shows a set of broad peaks (Figure 5). The broadening of the proton peaks in ^1H NMR studies of macrocycles is often a good indication of aggregation because

DOI: 10.1021/acs.inorgchem.7b00475
Inorg. Chem. XXXX, XXX, XXX−XXX

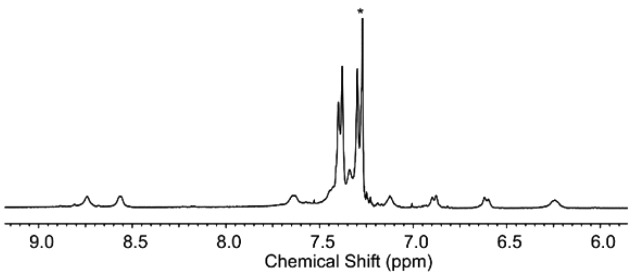

Figure 5. ^{1}H NMR spectrum of macrocycle **1a** in $CDCl_3$ at room temperature (400 MHz, c = 7.0 × 10^{-3} mol/L). Only the aromatic region is shown. *: $CHCl_3$ from the $CDCl_3$ solvent.

large aggregates have shorter T_2 relaxation times and macrocycles located in different environments within an aggregate are both effects that can lead to broadening.

To probe this further, we carried out a dilution experiment in $CDCl_3$ (Figure 6). At high concentration (7.3 × 10^{-3} mol/L),

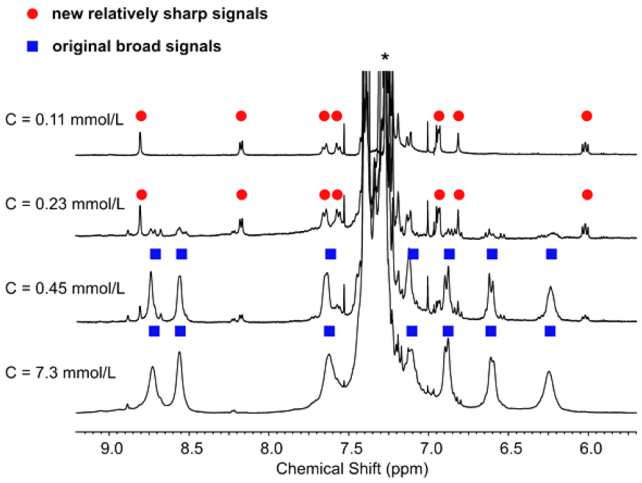

Figure 6. ^{1}H NMR spectra of macrocycle **1a** in $CDCl_3$ at different concentrations at room temperature (400 MHz). Only the aromatic region is shown. Blue squares indicate the original broad signals at high concentrations, and red circles indicate the new, relatively sharp signals at low concentrations.

the macrocycle only shows one set of major peaks that correspond reasonably well with those expected for macrocycle **1a**. After being diluted by 16 times (to 4.5 × 10^{-4} mol/L), a new set of sharper peaks are observed, with the original peaks remaining. With further dilution, this new set of peaks grows at the expense of the original set of broad peaks. At low concentration (1.1 × 10^{-4} mol/L), the original broad signals disappeared and only the new, relatively sharp peaks were present. This dilution experiment not only confirms the aggregation of macrocycle **1a** in $CDCl_3$ at room temperature but also suggests that the aggregation process is slow compared to the NMR time scale because both aggregates and monomer could be simultaneously resolved.

We attempted to investigate the aggregation behavior of macrocycle **1a** by dynamic light scattering and boiling-point-elevation measurements. However, these measurements gave unreliable results owing to the limited concentration ranges and low sensitivity. UV−vis spectroscopy of the macrocycle showed no deviation from Beer's law at concentrations below 10^{-4} mol/L (Figure S30), indicating that the macrocycle does not aggregate at these low concentrations. Therefore, to further study this aggregation, we performed a variable-temperature ^{1}H NMR study of macrocycle **1a** (Figure 7). Upon cooling of the

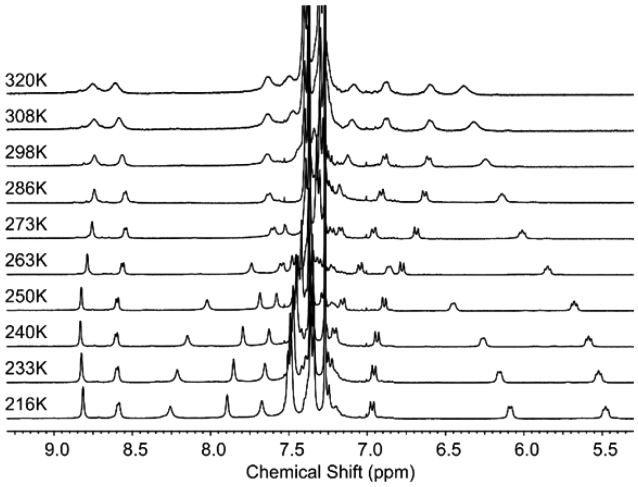

Figure 7. Variable-temperature ^{1}H NMR spectra of macrocycle **1a** in $CDCl_3$ (400 MHz, c = 7.0 × 10^{-3} mol/L). Only the aromatic region is shown.

sample, the peaks significantly sharpened and underwent large changes in chemical shift. Notably, the peak observed at ∼6.2 ppm shifted upfield as the sample was cooled, to a value closer to that of the monomer. Also, J coupling of this peak and others became evident as the sample was cooled. Our interpretation of these data is that the macrocycles are aggregated at room temperature (dimers, trimers, maybe larger) but dissociate upon cooling. This is characteristic of entropy-driven aggregation, as was previously observed in the cases of the Pt_4 rings and Zn_7/Cd_7 cluster complexes.[29] Thus, aggregation of the macrocycles results in desolvation and, consequently, an increase in the entropy. Lowering the temperature therefore favors disaggregation, resulting in sharper peaks.

To help understand the behavior of Pt_3 macrocycles in solution and to investigate these unusual NMR results, model compound **1c′** was synthesized. Scheme S2 shows the synthetic route to model compound **1c′**. Compound **1c′** was designed to have chemical shifts similar to those of macrocycle **1a**. To prevent cyclization, the pyridyl group was replaced by a phenyl ring.

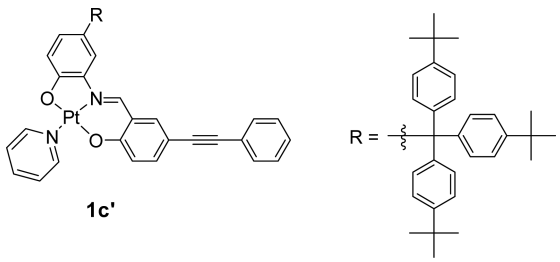

When model compound **1c′** was dissolved in $CDCl_3$, it showed a set of sharp peaks in the ^{1}H NMR spectrum. Dilution experiments with **1c′** were conducted and are shown in Figure S25. Different from **1a**, which demonstrated a conversion between two sets of peaks during dilution, model compound **1c′** only showed one set of peaks in the ^{1}H NMR spectrum at different concentrations. Also, chemical shift changes were minimal, indicating no self-association in this concentration

DOI: 10.1021/acs.inorgchem.7b00475
Inorg. Chem. XXXX, XXX, XXX−XXX

range. Thus, macrocycle **1a** aggregates when concentrated, but compound **1c′** does not.

In order to determine the size of the aggregates in solution at different temperatures, diffusion ordered spectroscopy (DOSY) was conducted at 298 and 250 K. Because the experiment depends on the viscosity of the solution (see the Supporting Information for details) and the viscosity depends on the temperature, we incorporated compound **1c′** as a reference.[30] A variable-temperature ^{1}H NMR study of compound **1c′** between 298 and 250 K showed no significant changes (Figure S26). This suggests that the size of compound **1c′** does not change much over this temperature range.

DOSY showed that the relative size of macrocycle **1a** (vs **1c′**) decreases as the temperature is lowered. Considering that the size of **1c′** does not change much with the temperature and when any interactions between **1a** and the reference compound are neglected, these data suggest that the size of the aggregates of macrocycle **1a** decrease as the temperature is lowered, consistent with our interpretation of the variable-temperature ^{1}H NMR data for **1a**.

A nuclear Overhauser effect NMR spectroscopy (NOESY) study of macrocycle **1a** in $CDCl_3$ was also conducted to probe its aggregation state. To study the distances between certain protons in macrocycle **1a**, the ^{1}H NMR peaks need to be assigned to individual protons. Because several peaks of **1a** overlapped at room temperature, which caused difficulties in peak assignment, we studied the macrocycle's behavior at lower temperatures. With the aid of HSQC [^{1}H and ^{13}C] and HMBC [^{1}H and ^{13}C], peaks at 240 K were assigned (Figure 8). The 2D NOESY NMR spectrum of **1a** at 240 K is shown in Figure 9.

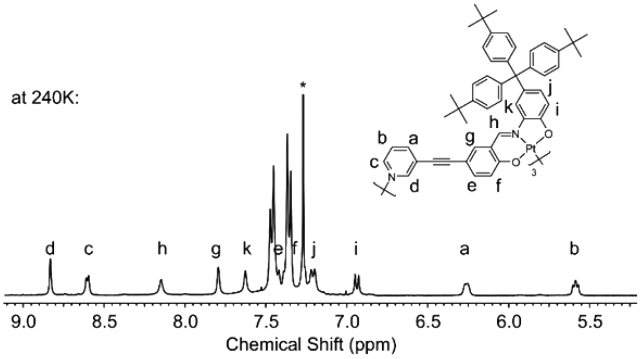

Figure 8. Aromatic region of the ^{1}H NMR spectrum of macrocycle **1a** in $CDCl_3$ with peak assignments (400 MHz, $c = 7.0 \times 10^{-3}$ mol/L, T = 240 K).

By using the previously calculated conformation of the macrocycle (Figure 3b), the expected distances between some protons could be calculated (Table 1). Although the distance between two types of protons have three different values in one macrocycle due to the 3-fold symmetry, only the closest value is listed in the table.

With protons b and c as the reference protons, the distance between the many protons could be estimated from their integral intensities (see Table 1 and the Supporting Information for details). For example, the estimated distance between protons g and h is about 2.36 Å, which is consistent with the expected value (2.24 Å). Notably, the distance between protons a and h is about 3.34 Å, which is very close to the distance between protons a and g (3.35 Å). However, the distance between protons a and k (3.21 Å) is much smaller than

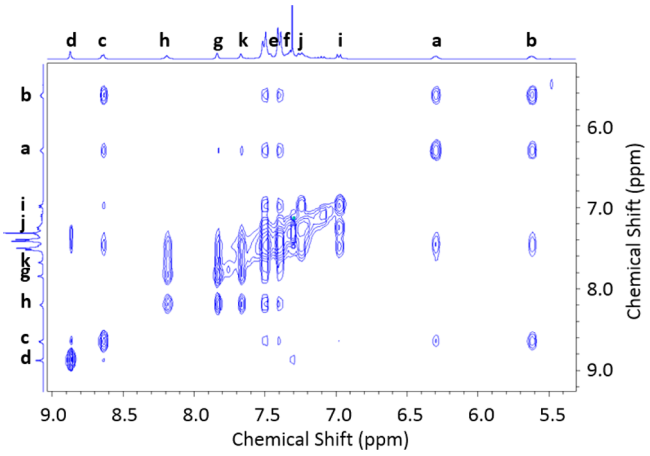

Figure 9. 2D NOESY NMR spectrum of macrocycle **1a** in $CDCl_3$ at 240 K (400 MHz, mixing time 0.1 s). Only the aromatic region is shown.

Table 1. Relative Integral and Estimated Distance Data from a NOESY NMR Study of Macrocycle 1a at 240 K

H^1	H^2	relative integral	relative distance	estimated closest distance[b]/Å	expected closest distance[a]/Å
b	c	1.00	1.00	2.51	2.51
a	b	1.02	1.00	2.51	2.51
h	g	1.67	0.92	2.30	2.24
h	k	2.40	0.86	2.17	2.05
a	g	0.12	1.42	3.57	5.10
a	h	0.11	1.44	3.63	7.20
a	k	0.21	1.30	3.26	8.58

[a]The expected distance was measured from one single macrocycle with optimized geometry (Figure 3b). [b]The estimated distance was calculated from the relative distance assuming r_{bc} = 2.51 Å.

the expected intramolecular value (8.58 Å). Similar unusually strong dipolar interactions such as a_{bg}, a_{bh}, and a_{bk} should not be observed within a single macrocycle.

Considering that macrocycle **1a** has a very rigid framework and is impossible to fold, these surprisingly strong coupling signals likely arise from the stacking of macrocycle **1a**. When stacked, pairs of protons are in closer proximity, leading to stronger dipolar coupling (Figure 10). Protons a and h from the same macrocycle (labeled with the same color) are too far apart to offer NOESY signals. The observed nuclear Overhauser effects are due to dipolar interaction between protons from different macrocycles (interaction between green and light-blue protons).

This stacking behavior also explains the coupling between protons a/b and aromatic protons from substituents R, which are far apart in a single macrocycle. In addition, because the distances r_{ag}, r_{ah}, and r_{ak} show similarly high values, it is likely that one macrocycle stacks on top of another macrocycle with proton a located close to protons g, h, and k from another macrocycle. Moreover, the similar values of the distances r_{ag}, r_{ah}, and r_{ak} are not consistent with a fixed conformation of aggregates, which implies that the relative twisting angle between two stacked adjacent macrocycles varies within a stack.[31] Notably, the unexpectedly short distances such as r_{ag} and r_{ah} are between 3.3 and 3.8 Å, consistent with typical π−π-stacking distances.[32]

For the purpose of comparing the aggregation behavior at room temperature with the behavior at low temperature,

DOI: 10.1021/acs.inorgchem.7b00475
Inorg. Chem. XXXX, XXX, XXX−XXX

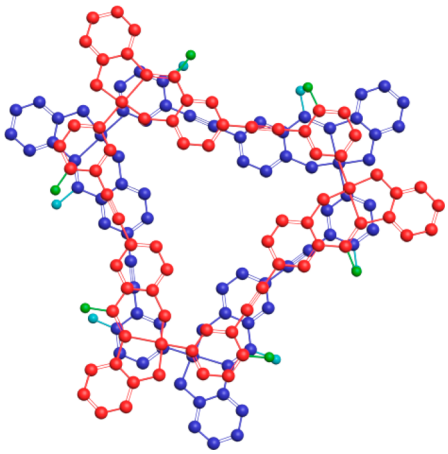

Figure 10. Top view of two stacked macrocycles **1a**, where the macrocycles have opposite orientations. Only protons a and h from different macrocycles are shown in green and light-blue color; other protons and R groups are removed for clarity.

NOESY NMR of macrocycle **1a** at room temperature was also performed. Due to overlapping peaks at room temperature, however, not all signals in its ^{1}H NMR spectrum could be assigned; peak overlap also caused trouble in the assignment of the coupling signals between 7.2 and 7.5 ppm in the 2D NOESY NMR spectrum. Hence, less data could be used for distance estimation in this case. Figure S29 shows the NOESY NMR spectrum of macrocycle **1a** at room temperature. Despite coupling of the signals between 7.2 and 7.5 ppm, calculation was conducted to estimate the distances between some protons (Table S3). The observation of cross-peaks for protons that are expected to be far from one another within a single macrocycle is evidence for aggregation at room temperature.

NOESY experiments showed that Pt_3 macrocycle **1a** displays aggregation in solution over a wide temperature range. Both the larger stack size from DOSY experiments and the broadening of ^{1}H NMR signals at higher temperature indicate that macrocycle **1a** has larger size at relatively higher temperature. This trend indicates that the self-assembly of Pt_3 macrocycles is entropy-driven, which is similar to Pt_4 macrocycles. Because aggregation of Pt_3 macrocycles causes a decrease of the particle numbers, this self-assembly process is believed to be a solvent-driven process.

■ CONCLUSIONS

In summary, we report an approach to tune both the geometry and size of platinum-containing macrocycles by inserting acetylene groups into pyridylsalicylaldimine ligands. Expanding organic linkers by introducing acetylene groups led to changes in both the size and geometry of macrocycles. The geometry change from 4-fold to 3-fold symmetry reduced the steric interaction between bulky substituent groups. As a result, Pt_3 macrocycles demonstrate comparably enhanced stacking. The self-assembly of platinum macrocycles in the solid state was studied with MALDI-TOF, PXRD, and TEM. Experiments showed that Pt_3 macrocycles stack into nanotubes in the solid state.

In addition, NMR spectroscopy was applied to study macrocycles' self-association in solution. Aggregates of Pt_3 macrocycles showed a decrease in size at lower temperatures, indicating that this self-assembly is an entropy-driven process. The conformation and aggregation of Pt_3 macrocycles was analyzed by a combination of computation, UV−vis experiments, variable-temperature NMR, and DOSY and NOESY NMR. These results challenge our design principles for platinum-containing macrocycles, and they may be useful for constructing molecule-based nanotubes and discotic liquid crystals.

■ ASSOCIATED CONTENT

Supporting Information

The Supporting Information is available free of charge on the ACS Publications website at DOI: 10.1021/acs.inorgchem.7b00475.

Syntheses, characterization, and calculations (PDF)

■ AUTHOR INFORMATION

Corresponding Author

*E-mail: mmaclach@chem.ubc.ca.

ORCID

Mark J. MacLachlan: 0000-0002-3546-7132

Author Contributions

The manuscript was written through contributions of all authors.

Notes

The authors declare no competing financial interest.

■ ACKNOWLEDGMENTS

We thank the Natural Sciences and Engineering Research Council of Canada for funding (Discovery Grant).

■ REFERENCES

(1) Lehn, J.-M. Supramolecular Chemistry. *Science* **1993**, *260*, 1762−1763.

(2) (a) Li, H.; Eddaoudi, M.; O'Keeffe, M.; Yaghi, O. M. Design and Synthesis of an Exceptionally Stable and Highly Porous Metal-Organic Framework. *Nature* **1999**, *402*, 276−279. (b) Eddaoudi, M.; Kim, J.; Rosi, N.; Vodak, D.; Wachter, J.; O'Keeffe, M.; Yaghi, O. M. Systematic Design of Pore Size and Functionality in Isoreticular MOFs and Their Application in Methane Storage. *Science* **2002**, *295*, 469−472. (c) Rosi, N. L.; Eckert, J.; Eddaoudi, M.; Vodak, D. T.; Kim, J.; O'Keeffe, M.; Yaghi, O. M. Hydrogen Storage in Microporous Metal-Organic Frameworks. *Science* **2003**, *300*, 1127−1129. (d) Férey, G.; Mellot-Draznieks, C.; Serre, C.; Millange, F.; Dutour, J.; Surblé, S.; Margiolaki, I. A Chromium Terephthalate-Based Solid with Unusually Large Pore Volumes and Surface Area. *Science* **2005**, *309*, 2040−2042.

(3) (a) Collier, C. P.; Mattersteig, G.; Wong, E. W.; Luo, Y.; Beverly, K.; Sampaio, J.; Raymo, F. M.; Stoddart, J. F.; Heath, J. R. A [2]Catenane-Based Solid State Electronically Reconfigurable Switch. *Science* **2000**, *289*, 1172−1175. (b) Leigh, D. A.; Wong, J. K. Y.; Dehez, F.; Zerbetto, F. Unidirectional Rotation in a Mechanically Interlocked Molecular Rotor. *Nature* **2003**, *424*, 174−179. (c) Hernández, J. V.; Kay, E. R.; Leigh, D. A. A Reversible Synthetic Rotary Molecular Motor. *Science* **2004**, *306*, 1532−1537. (d) Wilson, M. R.; Solà, J.; Carlone, A.; Goldup, S. M.; Lebrasseur, N.; Leigh, D. A. An Autonomous Chemically Fuelled Small-Molecule Motor. *Nature* **2016**, *534*, 235−240.

(4) (a) Krieg, E.; Shirman, E.; Weissman, H.; Shimoni, E.; Wolf, S. G.; Pinkas, I.; Rybtchinski, B. Supramolecular Gel Based on a Perylene Diimide Dye: Multiple Stimuli Responsiveness, Robustness, and Photofunction. *J. Am. Chem. Soc.* **2009**, *131*, 14365−14373. (b) Sahoo, P.; Sankolli, R.; Lee, H.-Y.; Raghavan, S. R.; Dastidar, P. Gel Sculpture: Moldable, Load-Bearing and Self-Healing Non-Polymeric Supramolecular Gel Derived from a Simple Organic Salt. *Chem. - Eur. J.* **2012**, *18*, 8057−8063. (c) Meazza, L.; Foster, J. A.; Fucke, K.; Metrangolo, P.; Resnati, G.; Steed, J. W. Halogen-Bonding-Triggered

DOI: 10.1021/acs.inorgchem.7b00475
Inorg. Chem. XXXX, XXX, XXX−XXX

Supramolecular Gel Formation. *Nat. Chem.* **2013**, *5*, 42−47. (d) Dong, S.; Yuan, J.; Huang, F. A Pillar[5]arene/Imidazolium [2]Rotaxane: Solvent- and Thermo-Driven Molecular Motions and Supramolecular Gel Formation. *Chem. Sci.* **2014**, *5*, 247−252.

(5) (a) Pedersen, C. J. Cyclic Polyethers and Their Complexes with Metal Salts. *J. Am. Chem. Soc.* **1967**, *89*, 7017−7036. (b) Pedersen, C. J. The Discovery of Crown Ethers (Noble Lecture). *Angew. Chem., Int. Ed. Engl.* **1988**, *27*, 1021−1027.

(6) (a) Staab, H. A.; Neunhoeffer, K. [2.2.2.2.2.2]Metacyclophane-1,9,17,25,33,41-hexayne from *m*-Iodophenylacetylene by Sixfold Stephens-Castro Coupling. *Synthesis* **1974**, *1974*, 424. (b) Moore, J. S.; Zhang, J. Efficient Synthesis of Nanoscale Macrocyclic Hydrocarbons. *Angew. Chem., Int. Ed. Engl.* **1992**, *31*, 922−924. (c) Gawroński, J.; Kolbon, H.; Kwit, M.; Katrusiak, A. Designing Large Triangular Chiral Macrocycles: Efficient [3 + 3] Diamine-Dialdehyde Condensations Based on Conformational Bias. *J. Org. Chem.* **2000**, *65*, 5768−5773. (d) Lee, S.; Chen, C.-H.; Flood, A. H. A Pentagonal Cyanostar Macrocycle with Cyanostilbene CH Donors Binds Anions and Forms Dialkylphosphate [3]Rotaxanes. *Nat. Chem.* **2013**, *5*, 704−710. (e) Li, Y.; Flood, A. H. Pure CH Hydrogen Bonding to Chloride Ions: A Preorganized and Rigid Macrocyclic Receptor. *Angew. Chem., Int. Ed.* **2008**, *47*, 2649−2652. (f) Liu, Y.; Singharoy, A.; Mayne, C. G.; Sengupta, A.; Raghavachari, K.; Schulten, K.; Flood, A. H. Flexibility Coexists with Shape-Persistence in Cyanostar Macrocycles. *J. Am. Chem. Soc.* **2016**, *138*, 4843−4851.

(7) (a) Zhang, J.; Moore, J. S. Liquid Crystals Based on Shape-Persistent Macrocyclic Mesogens. *J. Am. Chem. Soc.* **1994**, *116*, 2655−2656. (b) Höger, S.; Cheng, X. H.; Ramminger, A.-D.; Enkelmann, V.; Rapp, A.; Mondeshki, M.; Schnell, I. Discotic Liquid Crystals with an Inverted Structure. *Angew. Chem., Int. Ed.* **2005**, *44*, 2801−2805. (c) Stepien, M.; Donnio, B.; Sessler, J. L. Supramolecular Liquid Crystals Based on Cyclo[8]pyrrole. *Angew. Chem., Int. Ed.* **2007**, *46*, 1431−1435. (d) Kawano, S. -I; Hamazaki, T.; Suzuki, A.; Kurahashi, K.; Tanaka, K. Metal-Ion-Induced Switch of Liquid-Crystalline Orientation of Metallomacrocycles. *Chem. - Eur. J.* **2016**, *22*, 15674−15683.

(8) (a) Hui, J. K. H.; Frischmann, P. D.; Tso, C. H.; Michal, C. A.; MacLachlan, M. J. Spontaneous Hierarchical Assembly of Crown Ether-like Macrocycles into Nanofibers and Microfibers Induced by Alkali-Metal and Ammonium Salts. *Chem. - Eur. J.* **2010**, *16*, 2453−2460. (b) Ren, C.; Xu, S.; Xu, J.; Chen, X.; Zeng, H. Planar Macrocyclic Fluoropentamers as Supramolecular Organogelators. *Org. Lett.* **2011**, *13*, 3840−3843.

(9) (a) Forman, S. L.; Fettinger, J. C.; Pieraccini, S.; Gottarelli, G.; Davis, J. T. Toward Artificial Ion Channels: A Lipophilic G-Quadruplex. *J. Am. Chem. Soc.* **2000**, *122*, 4060−4067. (b) Sánchez-Quesada, J.; Isler, M. P.; Ghadiri, M. R. Modulating Ion Channel Properties of Transmembrane Peptide Nanotubes through Heteromeric Supramolecular Assemblies. *J. Am. Chem. Soc.* **2002**, *124*, 10004−10005. (c) Helsel, A. J.; Brown, A. L.; Yamato, K.; Feng, W.; Yuan, L.; Clements, A. J.; Harding, S. V.; Szabo, G.; Shao, Z.; Gong, B. Highly Conducting Transmembrane Pores Formed by Aromatic Oligoamide Macrocycles. *J. Am. Chem. Soc.* **2008**, *130*, 15784−15785. (d) Yan, X.; Xu, D.; Chen, J.; Zhang, M.; Hu, B.; Yu, Y.; Huang, F. A Self-Healing Supramolecular Polymer Gel with Stimuli-Responsiveness Constructed by Crown Ether Based Molecular Recognition. *Polym. Chem.* **2013**, *4*, 3312−3322.

(10) (a) Sanford, A. R.; Yuan, L.; Feng, W.; Yamato, K.; Flowers, R. A.; Gong, B. Cyclic Aromatic Oligoamides as Highly Selective Receptors for the Guanidinium Ion. *Chem. Commun.* **2005**, 4720−4722. (b) Liu, Y.; Shen, J.; Sun, C.; Ren, C.; Zeng, H. Intramolecularly Hydrogen-Bonded Aromatic Pentamers as Modularly Tunable Macrocyclic Receptors for Selective Recognition of Metal Ions. *J. Am. Chem. Soc.* **2015**, *137*, 12055−12063. (c) Xiao, D.; Zhang, D.; Chen, B.; Xie, D.; Xiang, Y.; Li, X.; Jin, W. Size-Selective Recognition by a Tubular Assembly of Phenylene-Pyrimidinylene Alternated Macrocycle through Hydrogen-Bonding Interactions. *Langmuir* **2015**, *31*, 10649−10655.

(11) (a) Fenniri, H.; Mathivanan, P.; Vidale, K. L.; Sherman, D. M.; Hallenga, K.; Wood, K. V.; Stowell, J. G. Helical Rosette Nanotubes: Design, Self-Assembly, and Characterization. *J. Am. Chem. Soc.* **2001**, *123*, 3854−3855. (b) Fenniri, H.; Deng, B.-L.; Ribbe, A. E. Helical Rosette Nanotubes with Tunable Chiroptical Properties. *J. Am. Chem. Soc.* **2002**, *124*, 11064−11072. (c) Zhang, W.; Moore, J. S. Arylene Ethynylene Macrocycles Prepared by Precipitation-Driven Alkyne Metathesis. *J. Am. Chem. Soc.* **2004**, *126*, 12796. (d) Zhang, W.; Moore, J. S. Reaction Pathways Leading to Arylene Ethynylene Macrocycles via Alkyne Metathesis. *J. Am. Chem. Soc.* **2005**, *127*, 11863−11870. (e) Pan, G.-B.; Cheng, X.-H.; Höger, S.; Freyland, W. 2D Supramolecular Structures of a Shape-Persistent Macrocycle and Co-deposition with Fullerene on HOPG. *J. Am. Chem. Soc.* **2006**, *128*, 4218−4219. (f) Ji, Q.; Le, H. T. M.; Wang, X.; Chen, Y.-S.; Makarenko, T.; Jacobson, A. J.; Miljanić, O. Š. Cyclotetrabenzoin: Facile Synthesis of a Shape-Persistent Molecular Square and Its Assembly into Hydrogen-Bonded Nanotubes. *Chem. - Eur. J.* **2015**, *21*, 17205−17209.

(12) (a) Lee, S.; Hirsch, B. E.; Liu, Y.; Dobscha, J. R.; Burke, D. W.; Tait, S. L.; Flood, A. H. Multifunctional Tricarbazolo Triazolophane Macrocycles: One-Pot Preparation, Anion Binding, and Hierarchical Self-Organization of Multilayers. *Chem. - Eur. J.* **2016**, *22*, 560−569. (b) Jester, S.-S.; Schmitz, D.; Eberhagen, F.; Höger, S. Self-Assembled Monolayers of Clamped Oligo(phenylene-ethynylene-butadiynylene)s. *Chem. Commun.* **2011**, *47*, 8838−8840.

(13) (a) Gallant, A. J.; MacLachlan, M. J. Ion-Induced Tubular Assembly of Conjugated Schiff-Base Macrocycles. *Angew. Chem., Int. Ed.* **2003**, *42*, 5307−5310. (b) Shimura, H.; Yoshio, M.; Kato, T. A Columnar Liquid-Crystalline Shape-Persistent Macrocycle Having a Nanosegregated Structure. *Org. Biomol. Chem.* **2009**, *7*, 3205−3207. (c) Cho, H.; Widanapathirana, L.; Zhao, Y. Water-Templated Transmembrane Nanopores from Shape-Persistent Oligocholate Macrocycles. *J. Am. Chem. Soc.* **2011**, *133*, 141−147. (d) Tzirakis, M. D.; Marion, N.; Schweizer, W. B.; Diederich, F. A Shape-Persistent Alleno-Acetylenic Macrocycle with a Modifiable Periphery: Synthesis, Chiroptical Properties and H-Bond-Driven Self-Assembly into a Homochiral Columnar Structure. *Chem. Commun.* **2013**, *49*, 7605−7607.

(14) (a) Shimizu, L. S.; Hughes, A. D.; Smith, M. D.; Davis, M. J.; Zhang, B. P.; zur Loye, H.-C.; Shimizu, K. D. Self-Assembled Nanotubes that Reversibly Bind Acetic Acid Guests. *J. Am. Chem. Soc.* **2003**, *125*, 14972−14973. (b) Bowers, C. R.; Dvoyashkin, M.; Salpage, S. R.; Akel, C.; Bhase, H.; Geer, M. F.; Shimizu, L. S. Crystalline Bis-urea Nanochannel Architectures Tailored for Single-File Diffusion Studies. *ACS Nano* **2015**, *9*, 6343−6353.

(15) Ono, K.; Tsukamoto, K.; Hosokawa, R.; Kato, M.; Suganuma, M.; Tomura, M.; Sako, K.; Taga, K.; Saito, K. A Linear Chain of Water Molecules Accommodated in a Macrocyclic Nanotube Channel. *Nano Lett.* **2009**, *9*, 122−125.

(16) Ren, C.; Maurizot, V.; Zhao, H.; Shen, J.; Zhou, F.; Ong, W.; Du, Z.; Zhang, K.; Su, H.; Zeng, H. Five-Fold-Symmetric Macrocyclic Aromatic Pentamers: High-Affinity Cation Recognition, Ion-Pair-Induced Columnar Stacking, and Nanofibrillation. *J. Am. Chem. Soc.* **2011**, *133*, 13930−13933.

(17) Shetty, A. S.; Zhang, J.; Moore, J. S. Aromatic π-Stacking in Solution as Revealed through the Aggregation of Phenylacetylene Macrocycles. *J. Am. Chem. Soc.* **1996**, *118*, 1019−1027.

(18) (a) Shimizu, L. S.; Smith, M. D.; Hughes, A. D.; Shimizu, K. D. Self-Assembly of a Bis-Urea Macrocycle into a Columnar Nanotube. *Chem. Commun.* **2001**, 1592−1593. (b) Shimizu, L. S.; Hughes, A. D.; Smith, M. D.; Samuel, S. A.; Ciurtin-Smith, D. Assembled Columnar Structures from Bis-Urea Macrocycles. *Supramol. Chem.* **2005**, *17*, 27−30.

(19) Ghadiri, M. R.; Granja, J. R.; Milligan, R. A.; McRee, D. E.; Khazanovich, N. Self-Assembling Organic Nanotubes Based on a Cyclic Peptide Architecture. *Nature* **1993**, *366*, 324−327.

(20) Yang, Y.; Feng, W.; Hu, J.; Zou, S.; Gao, R.; Yamato, K.; Kline, M.; Cai, Z.; Gao, Y.; Wang, Y.; Li, Y.; Yang, Y.; Yuan, L.; Zeng, X. C.;

DOI: 10.1021/acs.inorgchem.7b00475
Inorg. Chem. XXXX, XXX, XXX−XXX

Gong, B. Strong Aggregation and Directional Assembly of Aromatic Oligoamide Macrocycles. *J. Am. Chem. Soc.* **2011**, *133*, 18590−18593.

(21) (a) Moralez, J. G.; Raez, J.; Yamazaki, T.; Motkuri, R. K.; Kovalenko, A.; Fenniri, H. Helical Rosette Nanotubes with Tunable Stability and Hierarchy. *J. Am. Chem. Soc.* **2005**, *127*, 8307−8309. (b) Kim, H.-J.; Kang, S.-K.; Lee, Y.-K.; Seok, C.; Lee, J.-K.; Zin, W.-C.; Lee, M. Self-Dissociating Tubules from Helical Stacking of Noncovalent Macrocycles. *Angew. Chem., Int. Ed.* **2010**, *49*, 8471−8475. (c) Zhou, X.; Liu, G.; Yamato, K.; Shen, Y.; Cheng, R.; Wei, X.; Bai, W.; Gao, Y.; Li, H.; Liu, Y.; Liu, F.; Czajkowsky, D. M.; Wang, J.; Dabney, M. J.; Cai, Z.; Hu, J.; Bright, F. V.; He, L.; Zeng, X. C.; Shao, Z.; Gong, B. Self-Assembling Subnanometer Pores with Unusual Mass-Transport Properties. *Nat. Commun.* **2012**, *3*, 949. (d) Huang, Z.; Kang, S.-K.; Banno, M.; Yamaguchi, T.; Lee, D.; Seok, C.; Yashima, E.; Lee, M. Pulsating Tubules from Noncovalent Macrocycles. *Science* **2012**, *337*, 1521−1526.

(22) Frischmann, P. D.; Guieu, S.; Tabeshi, R.; MacLachlan, M. J. Columnar Organization of Head-to-Tail Self-Assembled Pt_4 Rings. *J. Am. Chem. Soc.* **2010**, *132*, 7668−7675.

(23) Frischmann, P. D.; Sahli, B. J.; Guieu, S.; Patrick, B. O.; MacLachlan, M. J. Sterically-Limited Self-Assembly of Pt_4 Macrocycles into Discrete Non-Covalent Nanotubes: Porous Supramolecular Tetramers and Hexamers. *Chem. - Eur. J.* **2012**, *18*, 13712−13721.

(24) For other papers reporting trinuclear platinum-containing macrocycles, see: (a) Yamamoto, T.; Arif, A. M.; Stang, P. J. Dynamic Equilibrium of a Supramolecular Dimeric Rhomboid and Trimeric Hexagon and Determination of Its Thermodynamic Constants. *J. Am. Chem. Soc.* **2003**, *125*, 12309−12317. (b) Bar, A. K.; Chakrabarty, R.; Chi, K.-W.; Batten, S. R.; Mukherjee, P. S. Synthesis and Characterisation of Heterometallic Molecular Triangles Using Ambidentate Linker: Self-Selection of a Single Linkage Isomer. *Dalton Trans.* **2009**, 3222−3229. (c) Ning, G.-H.; Xie, T.-Z.; Pan, Y.-J.; Li, Y.-Z.; Yu, S.-Y. Self-Assembly of Bowl-Like Trinuclear Metallo-Macrocycles. *Dalton Trans.* **2010**, *39*, 3203−3211.

(25) Thomas, R.; Lakshmi, S.; Pati, S. K.; Kulkarni, G. U. Role of Triple Bond in 1,2-Diphenylacetylene Crystal: A Combined Experimental and Theoretical Study. *J. Phys. Chem. B* **2006**, *110*, 24674−24677.

(26) Jiang, H.; Lin, W. Self-Assembly of Chiral Molecular Polygons. *J. Am. Chem. Soc.* **2003**, *125*, 8084−8085.

(27) Bühl, M.; Reimann, C.; Pantazis, D. A.; Bredow, T.; Neese, F. Geometries of Third-Row Transition-Metal Complexes from Density-Functional Theory. *J. Chem. Theory Comput.* **2008**, *4*, 1449−1459.

(28) Kline, M. A.; Wei, X.; Horner, I. J.; Liu, R.; Chen, S.; Chen, S.; Yung, K. Y.; Yamato, K.; Cai, Z.; Bright, F. V.; Zeng, X. C.; Gong, B. Extremely Strong Tubular Stacking of Aromatic Oligoamide Macrocycles. *Chem. Sci.* **2015**, *6*, 152−157.

(29) (a) Frischmann, P. D.; MacLachlan, M. J. Capsule Formation in Novel Cadmium Cluster Metallocavitands. *Chem. Commun.* **2007**, 4480−4482. (b) Frischmann, P. D.; Facey, G. A.; Ghi, P. Y.; Gallant, A. J.; Bryce, D. L.; Lelj, F.; MacLachlan, M. J. Capsule Formation, Carboxylate Exchange, and DFT Exploration of Cadmium Cluster Metallocavitands: Highly Dynamic Supramolecules. *J. Am. Chem. Soc.* **2010**, *132*, 3893−3908. (c) Frischmann, P. D.; Mehr, S. H. M.; Patrick, B. O.; Lelj, F.; MacLachlan, M. J. Role of Entropy and Autosolvation in Dimerization and Complexation of C_{60} by Zn_7 Metallocavitands. *Inorg. Chem.* **2012**, *51*, 3443−3453.

(30) Yao, S.; Howlett, G. J.; Norton, R. S. Peptide Self-Association in Aqueous Trifluoroethanol Monitored by Pulsed Field Gradient NMR Diffusion Measurements. *J. Biomol. NMR* **2000**, *16*, 109−119.

(31) (a) Sandström, J. *Dynamic NMR Spectroscopy*; Academic Press: London, 1982. (b) Gong, H.-Y.; Rambo, B. M.; Karnas, E.; Lynch, V. M.; Sessler, J. L. A 'Texas-Sized' Molecular Box that Forms an Anion-Induced Supramolecular Necklace. *Nat. Chem.* **2010**, *2*, 406−409.

(32) Janiak, C. A Critical Account on π-π Stacking in Metal Complexes with Aromatic Nitrogen-Containing Ligands. *J. Chem. Soc., Dalton Trans.* **2000**, 3885−3896.

DOI: 10.1021/acs.inorgchem.7b00475
Inorg. Chem. XXXX, XXX, XXX−XXX